

Formation Mechanism of Helical Polyacetylene with Spiral Morphology in Asymmetric Reaction Field Consisting of Chiral Nematic Liquid Crystal

Taizo Mori,[†] Mutsumasa Kyotani,[‡] and Kazuo Akagi^{*†}

[†]Department of Polymer Chemistry, Kyoto University, Kyoto 615-8510, Japan, and [‡]Tsukuba Research Center for Interdisciplinary Materials Science, University of Tsukuba, Ibaraki 305-8577, Japan

Received May 28, 2010; Revised Manuscript Received August 20, 2010

ABSTRACT: The formation mechanism of helical polyacetylene (H-PA) in chiral nematic liquid crystal (N*-LC) used as an asymmetric reaction field was investigated by taking into account the relationship in morphology between the H-PA and N*-LC. The spiral texture characteristic of N*-LC observed in polarized optical microscopy was examined and compared with the spiral morphology of the resultant H-PA. The distance between the fibril bundles of H-PA was determined to be half of a helical pitch of N*-LC; in addition, the helical axis of H-PA is orthogonal to that of N*-LC. Interestingly, the screw direction of the H-PA fibrils was found to be opposite to that of N*-LC. On the basis of these experimental facts, we propose a chemically graspable formation mechanism of H-PA in N*-LC.

1. Introduction

Helical conjugated polymers¹ are useful for various applications, such as nanowires,² electrical and magnetic devices,³ chiral resolution reagents,⁴ and biotechnologies.⁵ Polyacetylene (PA) is the simplest conjugated polymer and a prototype of an electrical conductive polymer.^{6–8} Because helical polyacetylene (H-PA) was synthesized in chiral nematic liquid crystal (N*-LC) used as an asymmetric reaction field,^{9,10} substituted PA derivatives of helical conformations have been extensively studied.^{4,11} The N*-LC can be prepared by adding a small amount of chiral compound as a chiral dopant into a nematic LC (N-LC).¹² The helical pitch of N*-LC is controlled by changing the helical twisting power and the concentration of the chiral dopant.¹³ The helical sense of N*-LC is regulated by the chirality of the chiral dopant. Therefore, the induction of chirality in N-LC with a chiral dopant is a type of chiral amplification.¹⁴ In addition, it was recently reported that helix formation is possible for not only PA but also other aromatic π -conjugated polymers without chiroptical substituents by using N*-LC as an asymmetric polymerization solvent.^{15,16}

Polarizing optical microscopy (POM) revealed a fingerprint texture of N*-LC and that the helical axis is in the plane of the plates.^{17,18} The H-PA domain contains a polydomain with spiral morphology, and each domain is composed of a fibril bundle with a one-handed screw direction.⁹ The spiral structure of H-PA is very similar to the spiral morphology of N*-LC, and it seems that the spiral morphology of H-PA is formed by replicating that of the N*-LC structure through interfacial acetylene polymerization. Although many studies have aimed to elucidate the formation mechanism of H-PA in the N*-LC, a thorough understanding is still lacking. It is essentially important for extending the versatility of the asymmetric polymerization using the N*-LC to rationalize unambiguously how the achiral monomer is polymerized to generate the helical conjugated polymer with a spiral morphology.

In this work, the structure of N*-LC was investigated with POM, and a model structure of the self-assembled N*-LC is proposed. The H-PA films synthesized in N*-LC as an asymmetric reaction field, and the morphologies of the films were investigated by

scanning electron microscopy (SEM). In addition, the relationship between the spiral structures of N*-LC and H-PA was elucidated. On the basis of experimental evidence, a chemically graspable description of the formation mechanism for H-PA in the N*-LC is proposed. The present formation mechanism should be applicable for other helical conjugated polymers synthesized in the asymmetric reaction fields consisting of N*-LCs or cholesteric LCs.

2. Experimental Section



2.1. Synthesis of N-LCs and Chiral Dopants. An N*-LC to be used as an asymmetric solvent was prepared by the addition of a small amount of chiral compound to an N-LC solution. To be the medium, the N*-LC must be chemically stable. Phenylcyclohexyl (PCH) derivatives, 4-(*trans*-4-*n*-propylcyclohexyl)-ethoxybenzene [PCH302] and 4-(*trans*-4-*n*-propylcyclohexyl)-butoxybenzene [PCH304] were synthesized by Williamson etherification. Molecular structures of these N-LCs are shown in Scheme S1 of the Supporting Information. The N phase of an equimolar mixture of two LCs, PCH302 and PCH304, was exhibited from 20 to 35 °C.

The mesophase temperature region of N*-LC depends on the concentration of the chiral dopant. With increasing concentration, the region narrows; in addition, the mesophase is destroyed when the concentration approaches a critical value. Because of the limitation of the concentration method, an alternative approach of using a chiral dopant with large twisting power was adopted. Axially chiral binaphthyl derivatives were used as chiral dopants because they have been reported to possess larger twisting powers than those of asymmetric carbon-containing chiral compounds. Binaphthyl derivatives, (*R*)- or (*S*)-1,1'-binaphthyl-2,2'-bis-[*para*-(*trans*-4-*n*-pentylcyclohexyl)phenolxy-1-hexyl]ether [(*R*)- or (*S*)-PCH506-Binol], were synthesized by Williamson etherification between chiroptical (*R*)- or (*S*)-1,1'-bi-2-naphthols and PCH derivatives. The substituent contains a PCH moiety, *n*-pentyl group (with five carbons), and a hexamethylene chain linked with an ether-type oxygen atom [-(CH₂)₆O-, 06] and is referred to as PCH506.

2.2. Preparation of N*-LC. We prepared the N*-LCs by adding 0.5 to 1.5 mol % of axially chiral binaphthyl derivatives [(*R*)- or (*S*)-PCH506-Binol] as chiral dopants to an equimolar mixture of the N-LCs, PCH302, and PCH304. The N*-LCs induced by (*R*)- and (*S*)-PCH506-Binol, which are abbreviated

*Corresponding author. E-mail: akagi@fps.polym.kyoto-u.ac.jp.

Table 1. Helical Pitches of N*-LCs and Interdistance of the Fibril Bundle of Helical Polyacetylene

n ^[a]	(R)-N*-LC		(R)-H-PA	
	Helical pitch ^[b] (μm)	Screw direction ^[c]	Distance between fibril bundles ($\pm 0.2 \mu\text{m}$)	Helical sense
1	9.1	 Right-handed	4.2	 Left-handed
2	4.6		2.4	
3	3.1		1.6	

^a Variable n is mole ratio of (R)-PCH506-Binol as chiral dopant [PCH302/PCH304/(R)-PCH506-Binol 100:100: n]. ^b Measured with Cano's wedge method at room temperature. ^c Determined with the contact method, in which cholesteryl oleyl carbonate is used as a standard N*-LC.

as (R)-N*-LC and (S)-N*-LC, respectively, exhibited fingerprint textures in POM. As shown in Figure S1 of the Supporting Information, the formation of an N*-LC was confirmed based on the appearance of Schlieren characteristics in the fingerprint texture by POM. The microscopic observation was carried out under crossed Nicol prisms with a Nikon ECLIPSE E 400 POL polarizing optical microscope equipped with a Nikon Coolpix 950 digital camera and a Linkam TH-600PM and L-600 heating and cooling stage with temperature control. Thermal transition behaviors were determined with a Perkin-Elmer differential scanning calorimeter (DSC) at a rate of $10^\circ\text{C min}^{-1}$ under an argon atmosphere. The temperature range of the N* phase was 14 to 32°C in the heating process and -12 to 31°C in the cooling process. Accounting for the effect of supercooling on the LCs, the catalyst solution consisting of the LC mixture and the chiral dopant was available for polymerization from 5 to 25°C . This sufficiently wide temperature region enabled us to perform the acetylene polymerization in the N* phase.

2.3. Synthesis of H-PA in N*-LC. The prepared N*-LCs were used as asymmetric solvents for a reaction with a Ziegler–Natta catalyst of $\text{Ti}(\text{O}-n\text{-Bu})_4$ and Et_3Al . The typical concentration of $\text{Ti}(\text{O}-n\text{-Bu})_4$ was 20 mmol/L, and the mole ratio of $[\text{Al}]/[\text{Ti}]$ was 4. The catalyst containing N*-LC was aged for 30 min at room temperature. During the aging, the catalyst containing N*-LC showed no noticeable change in optical texture and only a slight lowering of the transition temperature by 2 to 5°C , and thus the N*-LCs were confirmed to be chemically stable in the presence of the catalyst.

After aging, the N*-LC was moved via a syringe to a flat-bottomed container placed in a Schlenk flask. The Schlenk flask was connected to a vacuum line via a flexible joint and then degassed. We carried out the acetylene polymerization by introducing acetylene gas to the catalyst-containing N*-LC. The polymerization temperature was kept constant at 14°C to maintain the N* phase by circulating cooled ethanol through an outer flask enveloping the Schlenk flask. Acetylene gas (six-nine grade) was used without further purification. We maintained the polymerization temperature by immersing the Schlenk flask in a temperature-controlled alcohol bath. The initial acetylene pressure was about 20 to 30 Torr, and the polymerization time was 15 to 30 min. After polymerization, the PA film was washed with purified toluene several times and then with a 1 N HCl–methanol mixture and THF under argon at room temperature. The film was dried on a Teflon sheet through vacuum pumping and stored in a freezer at -20°C .

3. Results and Discussion

3.1. Characterization of N*-LC. The helical pitch (p) of the N*-LC was evaluated using Cano's wedged method.¹⁹ When the N*-LC sample was inserted into wedge-type cell with gradient thickness, the discontinuity lines named the Cano lines appeared on the surfaces of cell under crossed Nicols.^{20–22} We determined the helical pitch by measuring the distance (a) between Cano lines as follows: $p = 2a \tan \theta$, where θ is the angle of the wedge of the cell. Table 1 shows the changes of helical pitch

of the (R)-N*-LC as a function of mole ratio of the chiral dopant. For instance, when the concentrations of PCH302 and PCH304 and the chiral dopant were 100:100:1 in molar ratio, the concentration of the chiral dopant was 0.5 mol %, and the helical pitch of the (R)-N*-LC was evaluated to be $9.1 \mu\text{m}$. As the concentration of the chiral dopant increased, the helical pitch of the N*-LC decreased, indicating an increase in the degree of the helical twisting for the N*-LC.

Cholesteryl oleyl carbonate is known to be a left-handed N*-LC (cholesteric LC) and is useful as a standard LC in the miscibility test (contact method) for examining the helical sense of the N*-LC.²³ The miscibility test is based on the observation of the mixing area between the N*-LC and the standard LC using POM. When the screw direction of the N*-LC is the same as that of the standard LC, the mixing area is continuous; otherwise, it is discontinuous. As shown in Figure 1a, a mixture of (R)-N*-LC and cholesteryl oleyl carbonate exhibited a boundary of Schlieren texture in POM. In contrast, as shown in Figure 1b, a mixture of (S)-N*-LC and cholesteryl oleyl carbonate showed no change in the optical texture. These results demonstrate that the screw directions of (R)-N*-LC and (S)-N*-LC are opposite to and the same as that of cholesteryl oleyl carbonate, respectively. The (R)-N*-LC and (S)-N*-LC are right-handed and left-handed N*-LCs, respectively.

3.2. Model Structure of N*-LC. To gain insight into constructing a model of the N*-LC structure, we first examined how the spiral domain of the N*-LC changes under POM observation. Figures 2 and 3 show POM photographs of the N*-LC [PCH302/PCH304/(R)-PCH506-Binol 100:100:1] at a temperature close to the clearing point (34.5°C) between the N*-LC and isotropic phases. Movies of POM observations are also provided in the Supporting Information as Figures S2 and S3. Changes of the spiral domain spontaneously occurred upon a slight change in temperature around the clearing point. The domain grew from the center of the swirl and gradually increased in size, exhibiting a spiral texture with a left-handed direction (Figure 2). The newly formed spiral domain diminished in size by unfolding in the right-handed direction (Figure 3).

Figure 4 shows a POM photograph of the (R)-N*-LC domain that formed a left-handed double spiral structure. On the basis of this POM photograph, we proposed a model of the (R)-N*-LC domain, as shown in Figure 4. In our model, the spheroids are the N*-LC molecules, and the long axes of the spheroids are parallel to the director (an averaged direction for the LC molecules within a domain) of the N*-LC. The LC molecules are orthogonal to the chiral axis of the N*-LC, and the LC molecules rotate around the chiral axis of N*-LC. The double spiral is formed in the same direction as the N*-LC.

On the basis of our model, the (R)-N*-LC has a left-handed double spiral structure at the free surface, and the spatial period of the N*-LC is equal to one-half of the pitch. Therefore, the distance between the striae of the spiral domain corresponds to

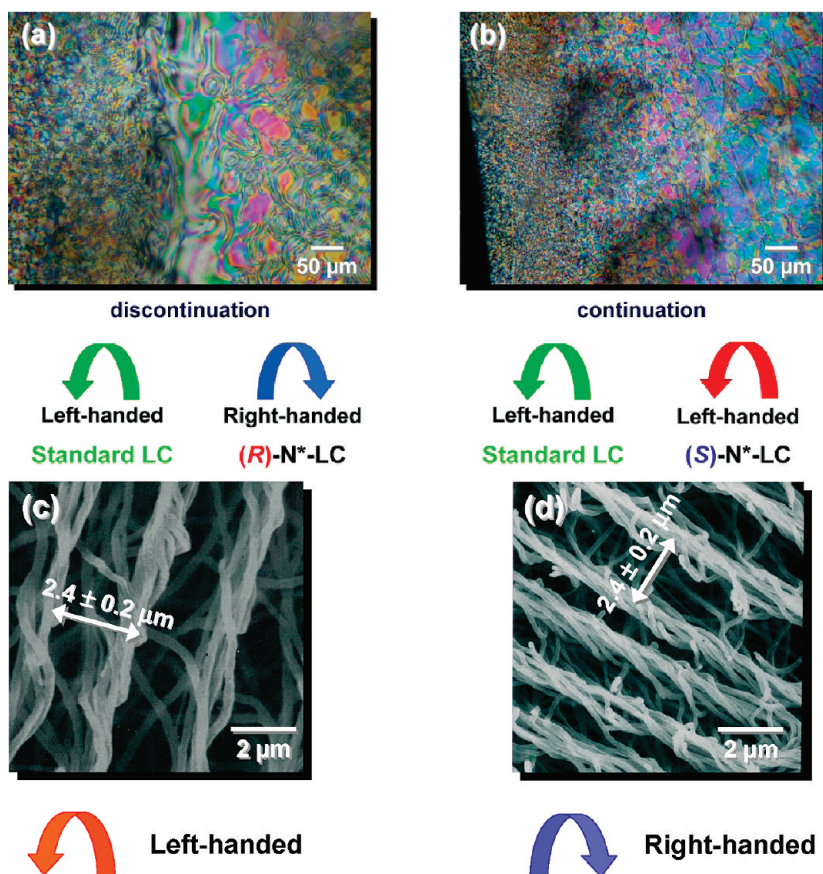


Figure 1. Miscibility tests between (a) (R)-N*-LC or (b) (S)-N*-LC and the standard LC (cholesteryl oleyl carbonate) with a left-handed screw direction at r.t. SEM images of fibril bundles of the H-PA film synthesized in (c) (R)-N*-LC and (d) (S)-N*-LC [PCH302/PCH304/(R)- or (S)-PCH506-Binol 100:100:2]. The distances of fibril bundles are $\sim 2.4 \mu\text{m}$, and the helical half pitch of (R)-N*-LC is $\sim 2.3 \mu\text{m}$.

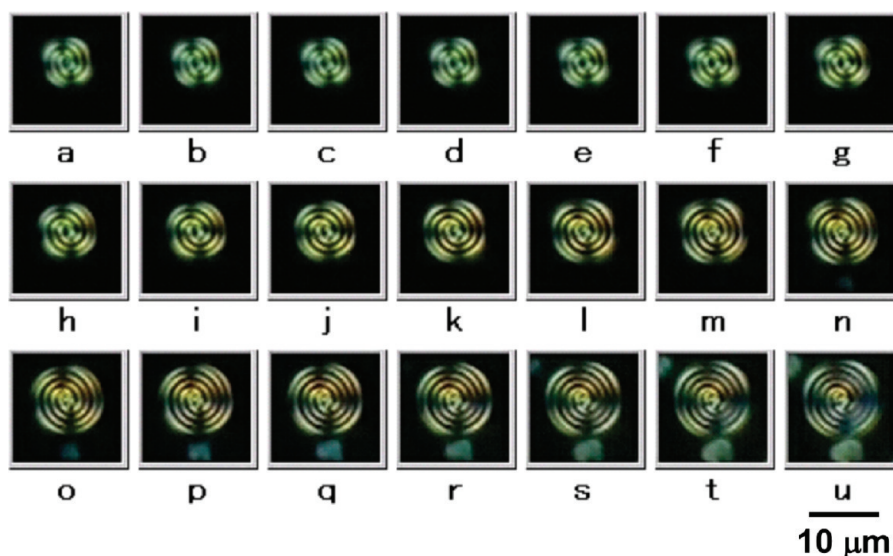


Figure 2. POM photographs of growing behaviors of (R)-N*-LC [PCH302/PCH304/(R)-PCH506-Binol 100:100:1] at 34.5°C in the cooling process from the isotropic to N*-LC phase. The temperature of 34.5°C corresponds to the clearing point between the N*-LC and isotropic phases.

one-half of the helical pitch of N*-LC. In the POM of the N*-LC domain, the dark and bright lines correspond to regions where N*-LC is perpendicular and parallel to the substrate, respectively. The helical axis of N*-LC is parallel to the substrate and expands from the center of the swirl.

3.3. Characterization of H-PA Films. The H-PA films synthesized in the (R)- and (S)-N*-LCs are abbreviated as (R)-H-PA and (S)-H-PA, respectively. The SEM images of

the H-PA films are shown in Figure 5. A polydomain with spiral morphology was formed with each domain composed of a helical bundle of fibrils with one-handed screw direction. The (R)-H-PA has a spiral morphology with a left-handed screw direction. The spiral direction of the H-PA synthesized in the N*-LC is the same as that of the N*-LC because the (R)-N*-LC showed a left-handed spiral structures. The polydomain-type fibril morphology of H-PA appears to

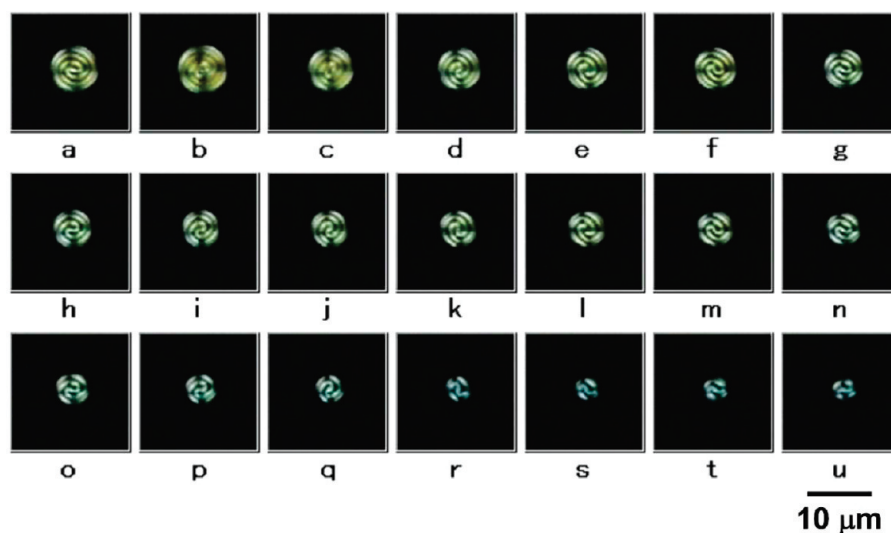


Figure 3. POM photographs of the diminishing behaviors of (R) -N*-LC [PCH302/PCH304/ (R) -PCH506-Binol 100:100:1] at 34.5 °C in the heating process from the N*-LC to isotropic phase. The temperature of 34.5 °C corresponds to the clearing point between the N*-LC and isotropic phases.

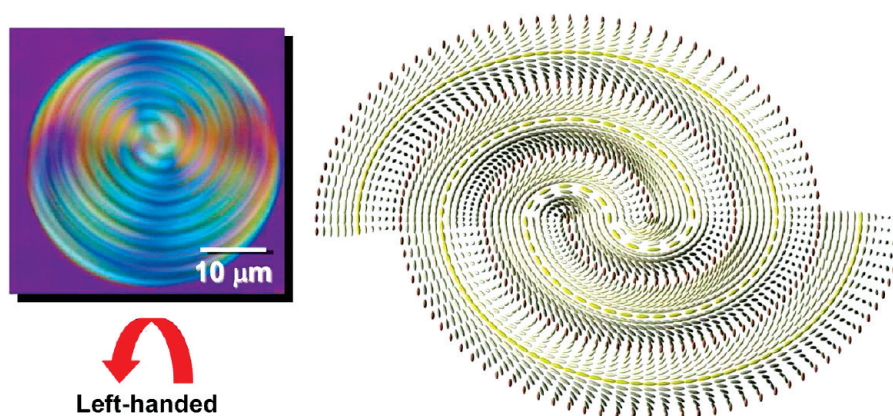


Figure 4. POM photograph of the spiral morphology of (R) -N*-LC at 14.0 °C and a model of the left-handed double spiral morphology of N*-LC.

replicate that of N*-LC during the interfacial acetylene polymerization.

As shown in Figure 1c,d, (R) -H-PA and the (S) -H-PA exhibited helical fibrillar morphologies with left- and right-handed screw directions, respectively. These results imply that the screw direction of H-PA is controlled by the helicity of the chiral dopant, that is, the optical configuration of the chiral dopant, so long as the N*-LC induced by the chiral dopant is employed as the asymmetric polymerization solvent. For (R) -H-PA, the fibrils screw in a left-handed manner, but the miscibility test showed that (R) -N*-LC has a right-handed helical structure (Figure 1a). Namely, the screw direction of the H-PA fibrils is opposite to that of the N*-LC used as the polymerization solvent. This was an unexpected result, especially to be solved unambiguously. (The more detailed arguments are cited in the Supporting Information. See also Figure S4, Table S1, and Schemes S2 and S3.)

As shown in Figures 1c,d, the fibril bundles of H-PA are aligned parallel to each other. Therefore, the distance between the fibril bundles remains unchanged. The morphology of the fibril bundles of H-PA is similar to the fingerprint texture observed in the N*-LC. We examined the distance between the fibril bundles of PA through magnified SEM images and compared it with the helical pitch of the N*-LC (Table 1). The distance between the fibril bundles of H-PA was 4.2 μm when the N*-LC with a helical pitch of 9.1 μm

was used as the asymmetric reaction field. The distance between the fibril bundles is equal to about one-half of the pitch of the corresponding N*-LC.

Figure 6 shows circular dichroism (CD) spectra of the H-PAs. Positive and negative Cotton effects for (R) - and (S) -H-PA were observed, respectively, in the region from 450 to 800 nm, corresponding to a $\pi \rightarrow \pi^*$ transition of the PA chain. These results indicated that the PA main chain is helically screwed, despite the absence of chiroptical side chains.

3.4. Formation Mechanism of the H-PA in the N*-LC.

Figure 7 shows a POM photograph of the spiral morphology of (S) -N*-LC and an SEM image of (S) -H-PA. The spiral morphology of H-PA resembles that of N*-LC. The relationship between the H-PA and the N*-LC is as follows: (i) The twist direction of (R) -N*-LC is right-handed, whereas the screw direction of the (R) -H-PA is left-handed. The screw direction of the H-PA fibrils is opposite to the twist direction of the N*-LC. (ii) The half-helical pitch (4.6 μm) of N*-LC is close to the distance between the H-PA fibril bundles (4.2 μm). (iii) The screw direction for H-PA having spiral morphology is the same as that of N*-LC. Therefore, the H-PA grows along with the striae of the fingerprint texture of N*-LC. As seen in Figure 7, the helical axis of H-PA is parallel to the PA chain, and the helical axis of N*-LC is perpendicular to the striae of the N*-LC. Therefore, the helical axis of H-PA is perpendicular to that of the N*-LC.

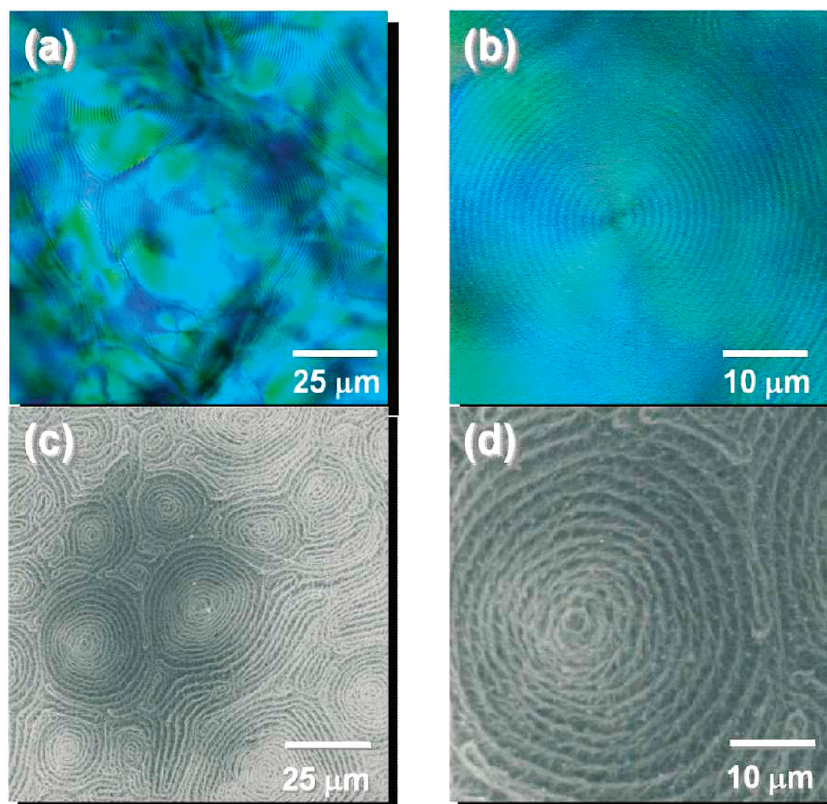


Figure 5. (a,b) POM photographs of spiral morphologies of (*R*)-N*-LC at 14.0 °C and (c,d) SEM images of hierarchical spiral morphologies of H-PA film synthesized in (*R*)-N*-LC [PCH302/PCH304/(*R*)-PCH506-Binol 100:100:3]. The distance between fibril bundles is $\sim 1.6 \mu\text{m}$, and the helical half pitch of (*R*)-N*-LC is $\sim 1.5 \mu\text{m}$. (See Figure 8, as for the helical half pitch of N*-LC.)

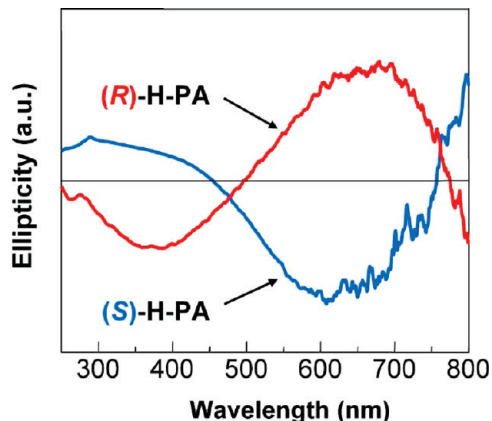


Figure 6. CD spectra of H-PA thin films ((*R*)-H-PA and (*S*)-H-PA) synthesized in (*R*)-N*-LC and (*S*)-N*-LC, respectively [PCH302/PCH304/(*R*)- or (*S*)-PCH506-Binol 100:100:3].

When discussing the formation mechanism of the H-PA in the N*-LC, we must consider the free surface structure of the N*-LC because the acetylene polymerization occurs interfacially between the gas and liquid phases. Experimental evidence from acetylene polymerizations using gravity flow and magnetic field methods^{24,25} revealed that the PA chains grow along the LC molecules. This is easily understood by viewing the external force-oriented LC reaction field, where the aligned LCs form so-called “one-directionally lined guardrails” and the PA chains are allowed to grow only along and between the guardrails, as shown in Figure S5 of the Supporting Information.

Therefore, the formation mechanism of the H-PA in the N*-LC was examined by accounting for both the acetylene polymerization process and the relationship between the

morphology of the H-PA and the helical structure of the N*-LC. Figure 8 shows a plausible mechanism for the interfacial acetylene polymerization in the N*-LC, which is based on the model structure of the N*-LC previously shown in Figure 4. In Figure 8, the H-PAs are represented as blue ribbons, and they are assumed to grow along the N*-LC molecules (yellow spheroids) horizontal to the substrate. The H-PA chains grow with a helically twisted structure and form helical fibrils through van der Waals interactions. The fibrils further gather to form a bundle of fibrils. (See Figure 12.) It is apparent from Figure 8 that the distance between the fibrils in a bundle corresponds to the helical pitch of the N*-LC. The helical axis of the N*-LC radiates in all directions out of the central vortex, whereas the H-PA helical axis is along the tangential line of the vortex. Therefore, the helical axes of the N*-LC and H-PA are orthogonal to each other.

In the case of right-handed N*-LC, the H-PA chain grows from the catalytic species in a left-handed manner. The distance of the H-PA fibrils corresponds to one-half of the pitch of N*-LC. Because it is difficult for PA to be orthogonal to the LC molecule, it grows parallel to the LC molecules. The helical axes of the H-PA are aligned parallel to the striae and thus the director of N*-LC. The director and the helical axis of N*-LC are perpendicular to each other. Therefore, the helical axis of PA is perpendicular to that of N*-LC. The H-PA chains with a screw direction opposite to that of N*-LC smoothly propagate along the LC molecules, as shown in Figure 9a. When the H-PA chains with the same screw direction as that of the N*-LC encounter the LC molecules, a sterically unfavorable polymerization results, as shown in Figure 9b.

The present polymerization mechanism for H-PA resembles that of a so-called “spiral bevel gear”,²⁷ as shown in Figure 10, in which two gears are orthogonally arranged with

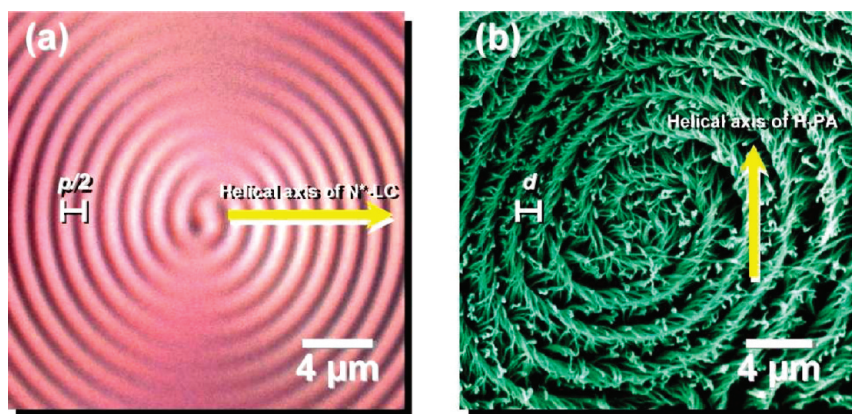


Figure 7. (a) POM photograph of spiral morphology of (S)-N*-LC, [PCH302/PCH304/(S)-PCH506-Binol 100:100:2] at 14.0 °C. (b) SEM image of spiral morphology of H-PA film. The helical half pitch ($p/2$) of (S)-N*-LC is $\sim 2.3 \mu\text{m}$, and the distance between the fibril bundles (d) is $\sim 2.4 \mu\text{m}$. The arrows in the Figures indicate (a) the helical axis of N*-LC and (b) the helical axis of H-PA.

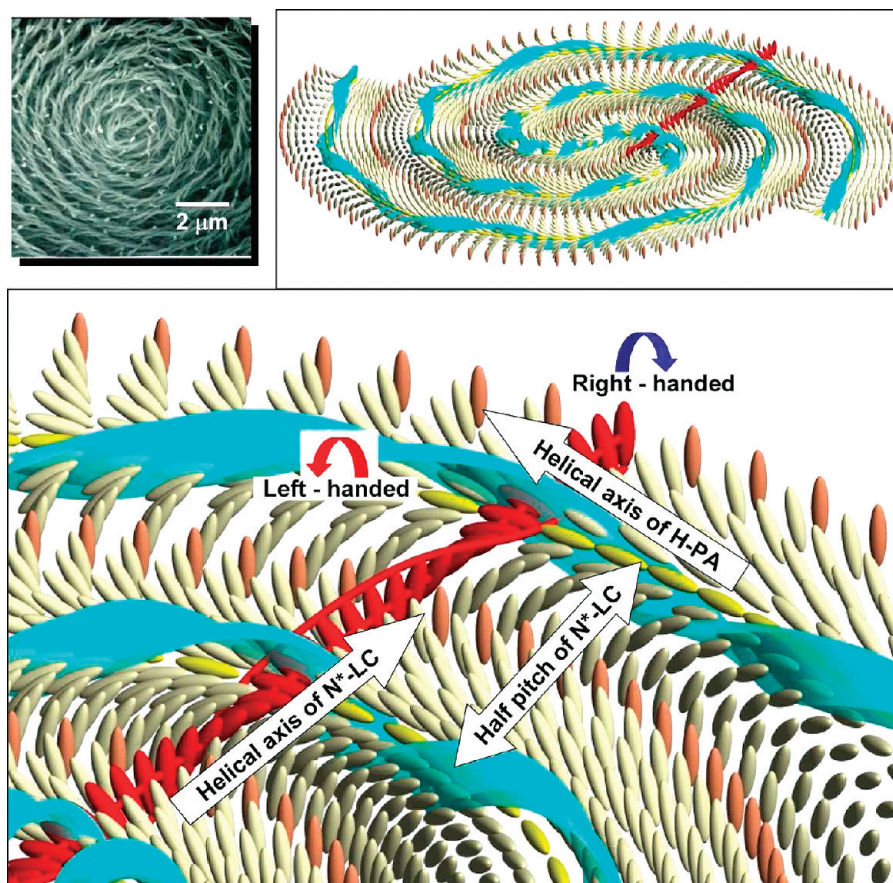


Figure 8. Schematic representation of the mechanism for acetylene polymerization in N*-LC (upper right and lower). H-PA chains with a left-handed screw direction grow and extend in the right-handed N*-LC. An SEM image of H-PA film is shown for comparison (upper left).

spiral directions opposite to each other. The rotation torque of the gear can be transferred to another gear with an opposite rotation direction. In the spiral bevel gear, two gears are set to be orthogonal, and their spiral rotation directions are opposite to each other. If the gears have the same spiral directions, then the rotation torque of one gear cannot be transferred to another one. Similarly, the spiral axis of the H-PA is orthogonal to that of the N*-LC, and hence the spiral directions need to be opposite to each other; otherwise, the H-PA cannot grow in the N*-LC. Hereafter, the present acetylene mechanism is called the “bevel-type screw arrangement” mechanism between the forming PA fibrils and the LC twist.

To prove the proposed formation mechanism more directly and evidently, we attempted to observe in stepwise the in-site growth of PA chains and fibril bundles by using CCD camera under POM. However, the in-site observation failed because (i) the interfacial acetylene polymerization is instantly completed, the speed of which is too fast to be observed by CCD camera, and (ii) the N*-LC including $\text{Ti}(\text{O}-n\text{-Bu})_4\text{-AlEt}_3$ catalyst is black in color, prohibiting the observation of the polymerization surface itself.

Therefore, instead we depicted a plausible overall acetylene polymerization in the N*-LC reaction field on the basis of the “bevel-type screw arrangement” mechanism. As shown in Figure 11, the PA chain grows along the twisted

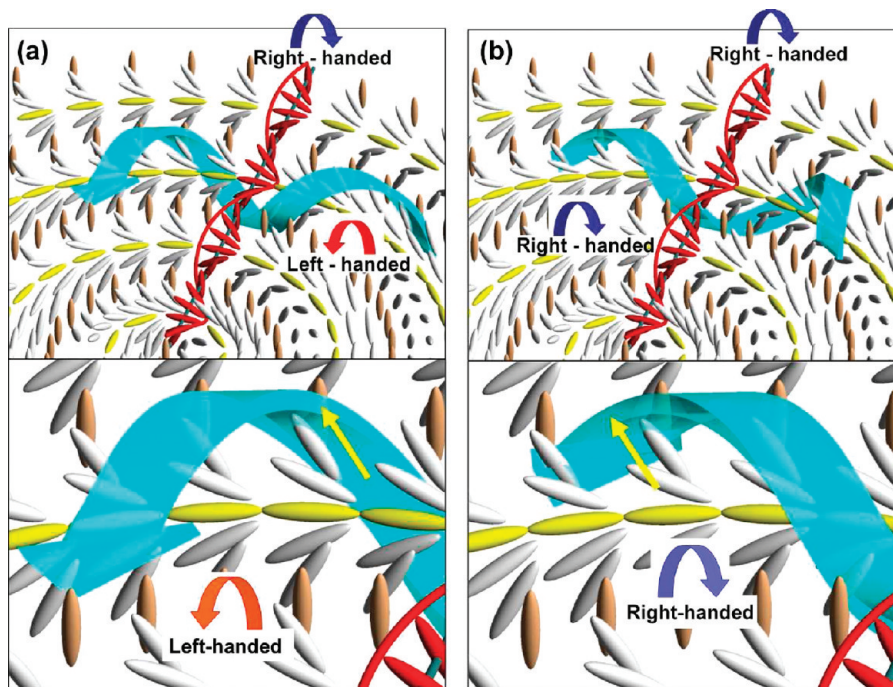


Figure 9. Schematic representation of the mechanism for acetylene polymerization in N*-LC. H-PAs with (a) left-handed and (b) right-handed screw directions are assumed to grow in the right-handed N*-LC. The PA chain can grow along the director of N*-LC when the helical direction of H-PA and the screw direction of the N*-LC are opposite to each other (a). However, the PA chain cannot grow along the director of N*-LC when the helical direction of PA is coincident with the N*-LC direction (b).

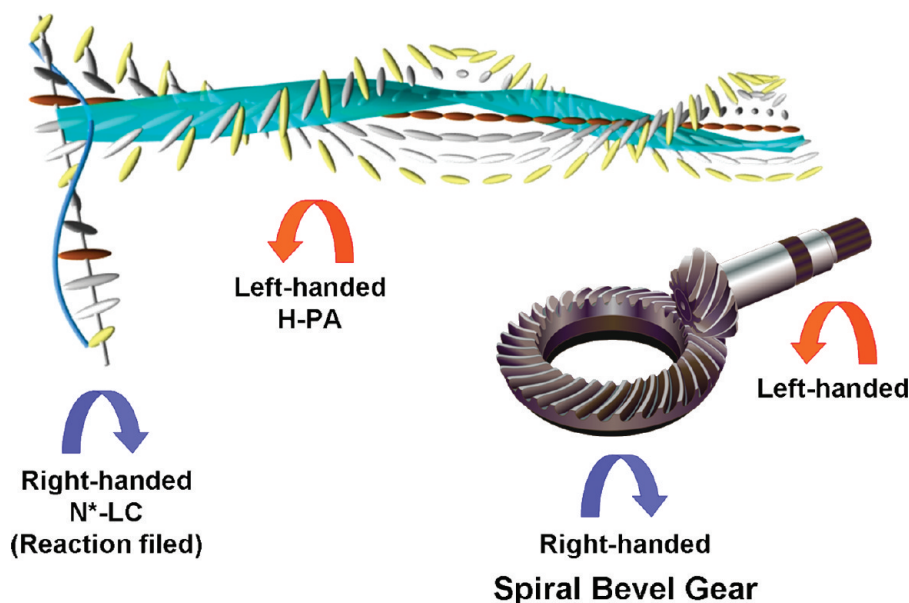


Figure 10. Relationship between helical axis of the N*-LC and that of H-PA and illustration of spiral bevel gear.²⁶

LC molecules, particularly around the LC molecules horizontally placed to the substrate to give a helical chain (a). Note that horizontally aligned LCs (represented by yellow) are much more favorable for the growing of PA chains than the vertically aligned ones (represented by red color) because the PA growth along the latter LC molecules needs the diffusion of acetylene into the N*-LC solution and becomes less active compared with the interfacial polymerization mainly contributed by horizontally placed LC molecules. The neighboring helical chains spontaneously form a helical fibril through van der Waals interaction (b). Besides, the neighboring helical fibrils are gathered through van der Waals forces to produce a bundle of fibrils with helically

twisted structure (c). Similar growths of helical PA chains, fibrils, and bundle of fibrils should occur simultaneously around the horizontally aligned LC molecules, which are separated by a half helical pitch of the N*-LC (d), and hence the bundles of fibrils are separated by a half helical pitch of the N*-LC (e). Because the horizontally aligned LC molecules exhibit a spiral structure, the bundle of fibrils also forms spiral morphology (f). The helical axes of N*-LC and H-PA are orthogonal to each other.

Figure 12 shows the superhierarchical helical structures in the H-PA. The H-PA main chain is twisted with a one-handed direction. There is also a screwed structure and a bundle of fibrils with the same screw direction as that of the

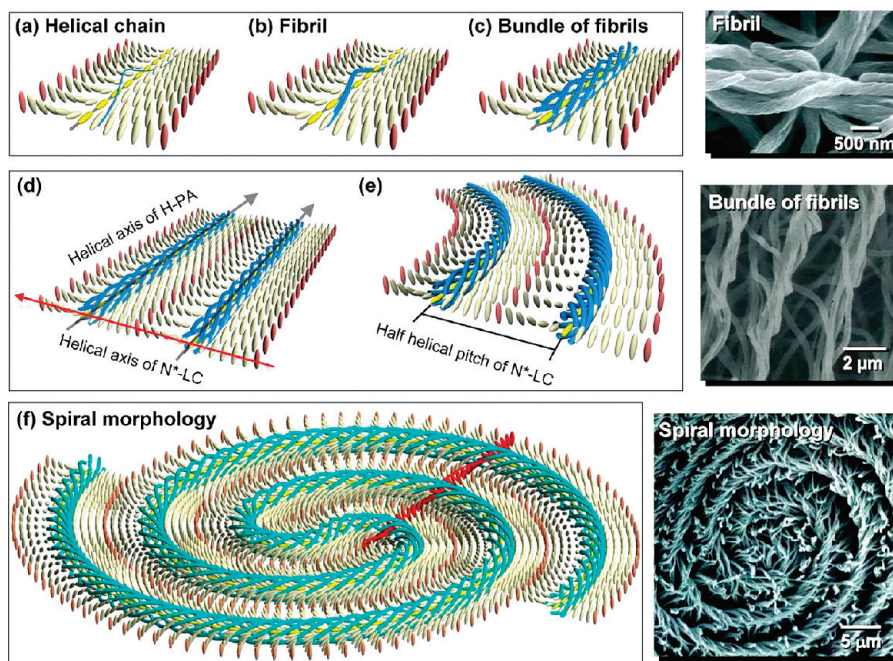


Figure 11. Plausible overall acetylene polymerization in the N^* -LC reaction field on the basis of the “bevel-type screw arrangement” mechanism.

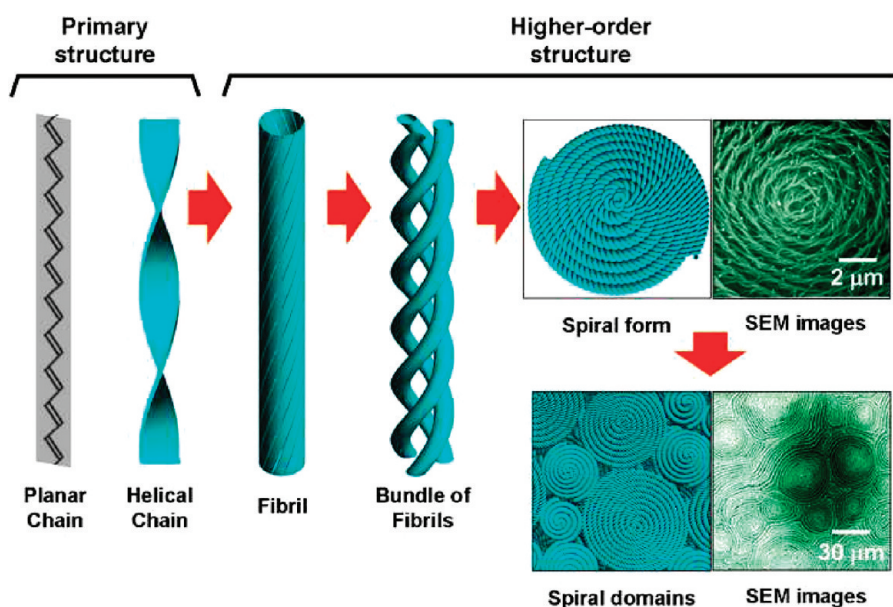


Figure 12. Hierarchical helical structures from the primary to the higher-order structure in helical polyacetylene.

fibril. The higher-order structure gives the characteristic spiral morphology, which is scarcely observed in synthetic polymers. Such a helical structure is due to the asymmetrical polymerization using the N^* -LC as a reaction field.

The present mechanism is also applicable for the acetylene polymerization in magnetically aligned N^* -LC.²⁷ When a magnetic field of 5 T was applied to the N^* -LC of polydomain structure, N^* -LC macroscopically aligned to form a monodomain structure (Figure 13a,b). The helical axis of N^* -LC is perpendicular to the direction of the magnetic field (Figure 13a). The acetylene polymerization in the N^* -LC of monodomain structure produces a macroscopically aligned H-PA. Whereas the helical axis of the fibril bundle of H-PA is parallel to the direction of the magnetic field, it is perpendicular to the helical axis of the

N^* -LC. Similarly to the case of the polydomain N^* -LC, the orthogonal relationship in the direction of the helical axis between the N^* -LC as a reaction field and the H-PA as a reaction product is observed in the monodomain reaction field. The polymerization results of Figure 13 are consistent with the results depicted in Figures 8, 9, and 11; the H-PAs grow along the N^* -LC molecules in each domain. Figure 14 shows a schematic representation of the acetylene polymerization in the macroscopically aligned N^* -LC with a monodomain structure. In this Figure, the H-PAs with a left-handed screw structure grow in the right-handed monodomain N^* -LC. The H-PAs are gathered through van der Waals interactions to form helical fibrils, and the helical fibrils further form helical fibril bundles to produce a macroscopically aligned morphology (Figure 13).

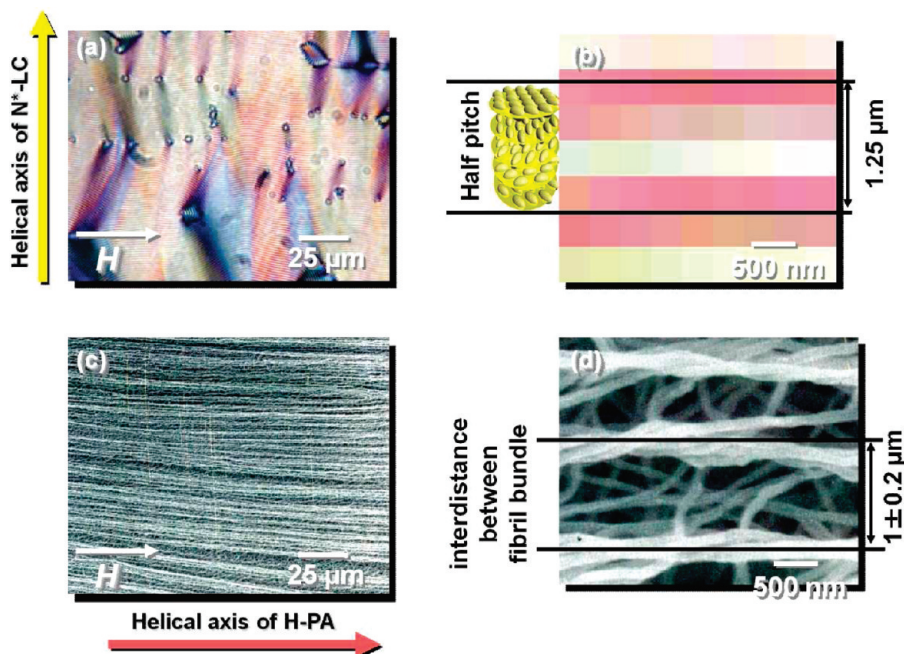


Figure 13. (a,b) POM photographs of N*-LC with a monodomain under a magnetic field of 5 T for 5 min at 14.0 °C. (c,d) SEM images of H-PA film synthesized in the aligned (R)-N*-LC with a monodomain under a magnetic field [PCH302/PCH304/(R)-PCH506-Binol 100:100:3 molar ratio].

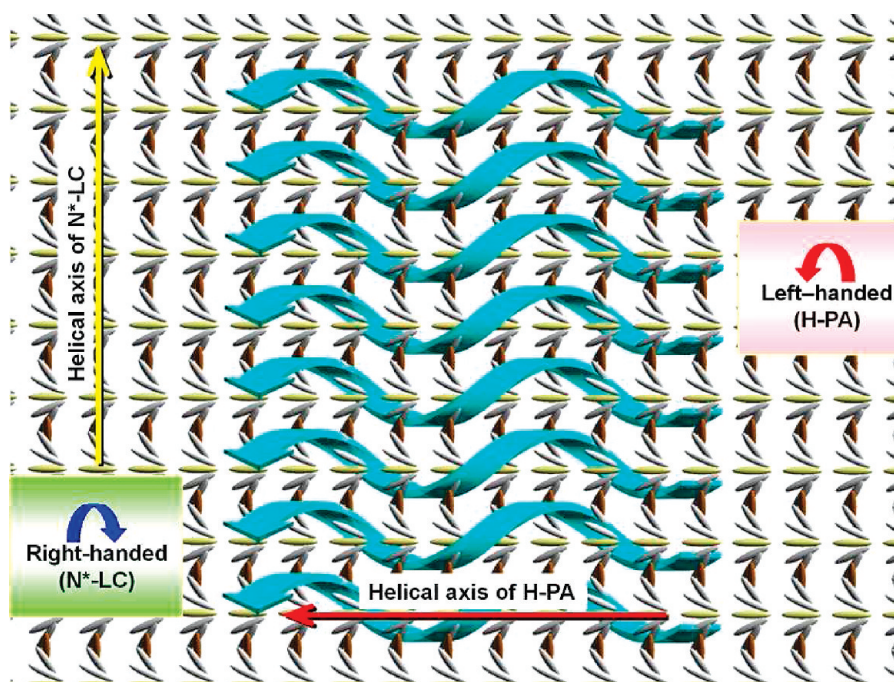


Figure 14. Schematic representation of the mechanism for acetylene polymerization in the macroscopically aligned N*-LC under a magnetic field. H-PAs with left-handed screw direction grow in the right-handed N*-LC. Helical axes of H-PA are perpendicular to those of N*-LC.

4. Conclusions

The formation mechanism of the H-PA in the N*-LC used as an asymmetric reaction field was clarified by taking into account the relationship in morphology between the N*-LC structure and the H-PA. The interdistance of the fibril bundles of the H-PA is nearly equal to the half helical pitch of the N*-LC. The helical axis of H-PA is orthogonal to that of the N*-LC. The helically twisted direction of the H-PA fibrils is opposite to that of the N*-LC. The model for the spiral morphology of N*-LC was presented, and the chemically graspable picture for the mechanism of the acetylene polymerization in the N*-LC was provided.

The present formation mechanism should be applicable for other helical conjugated polymers synthesized in the asymmetric reaction fields composed of N*-LCs or cholesteric LCs.

Acknowledgment. This work was supported by a Grant-in-Aid for Science Research (S) (no. 20225007) from the Ministry of Education, Culture, Sports, Science and Technology, Japan, and partially supported by Ogasawara Foundation for Science and Technology of Japan.

Supporting Information Available: Molecular structures of N-LCs, Schlieren and fingerprint textures observed in N-LCs

and N*-LCs, movies of POM observations, structures of cholesteryl chloride and cholesteryl oleyl carbonate, miscibility test between cholesteryl chloride or N*-LC induced by cholesteryl chloride and the standard LC (cholesteryl oleyl carbonate) with a left-handed screw direction between (R)-N*-LC and N*-LC induced by cholesteryl chloride, concentration dependence of screw direction of N*-LCs, arguments concerning the relationship between the helical twisting directions of the N*-LC and H-PA, and relationship between the helical twisting directions of the N*-LC and H-PA. This material is available free of charge via the Internet at <http://pubs.acs.org>.

References and Notes

- (1) Iwasaki, T.; Nishide, H. *Curr. Org. Chem.* **2005**, *9*, 1665.
- (2) (a) Lee, H. J.; Jin, Z. X.; Aleshin, A. N.; Lee, J. Y.; Goh, M. J.; Akagi, K.; Kim, Y. S.; Kim, D. W.; Park, Y. W. *J. Am. Chem. Soc.* **2004**, *126*, 16722. (b) Aleshin, A. N.; Lee, H. J.; Park, Y. W.; Akagi, K. *Phys. Rev. Lett.* **2004**, *93*, 196601. (c) Aleshin, A. N.; Lee, H. J.; Akagi, K.; Park, Y. W. *Microelectron. Eng.* **2005**, *81*, 420. (d) Aleshin, A. N.; Lee, H. J.; Jhang, S. H.; Kim, H. S.; Akagi, K.; Park, Y. W. *Phys. Rev. B* **2005**, *72*, 153202. (e) Lee, S. W.; Kim, B.; Lee, D. S.; Lee, H. J.; Park, J. G.; Ahn, S. J.; Campbell, E. B.; Park, Y. W. *Nanotechnology* **2006**, *17*, 992. (f) Ofuji, M.; Takano, Y.; Houkawa, Y.; Takanishi, Y.; Ishikawa, K.; Takezoe, H.; Mori, T.; Goh, M.; Guo, S.; Akagi, K. *Jpn. J. Appl. Phys.* **2006**, *45*, 1710.
- (3) (a) Langeveld-Voss, B. M. W.; Janssen, R. A. J.; Christiaans, M. P. T.; Meskers, S. C. J.; Dekkers, H. P. J. M.; Meijer, E. W. *J. Am. Chem. Soc.* **1996**, *118*, 4908. (b) Peeters, E.; Christiaans, M. P. T.; Janssen, R. A. J.; Schoo, H. F. M.; Dekkers, H. P. J. M.; Meijer, E. W. *J. Am. Chem. Soc.* **1997**, *119*, 9909.
- (4) (a) Yashima, E.; Maeda, K.; Okamoto, Y. *Nature* **1999**, *399*, 449. (b) Nakano, T.; Okamoto, Y. *Chem. Rev.* **2001**, *101*, 4013. (c) Yamamoto, C.; Okamoto, Y. *Bull. Chem. Soc. Jpn.* **2004**, *77*, 227. (d) Maeda, K.; Morino, K.; Okamoto, Y.; Sato, T.; Yashima, E. *J. Am. Chem. Soc.* **2004**, *126*, 4329.
- (5) (a) Bross, P. A.; Schoberl, U.; Daub, J. *Adv. Mater.* **1991**, *3*, 198. (b) Li, W.; Wang, H. L. *J. Am. Chem. Soc.* **2004**, *126*, 2278. (c) Iwaura, R.; Hoeben, F. J. M.; Masuda, M.; Schenning, A. P. H. J.; Meijer, E. W.; Shimizu, T. *J. Am. Chem. Soc.* **2006**, *128*, 13298.
- (6) *Handbook of Conducting Polymers*; Skotheim, T. A., Ed.; Marcel Dekker: New York, 1986.
- (7) *Handbook of Organic Conductive Molecules and Polymers*; Nalwa, H. S., Ed.; Wiley: New York, 1997.
- (8) Akagi, K.; Shirakawa, H. Fundamentals, Methods, and Applications. In *Electrical and Optical Polymer Systems*; Wise, D. L.; Wnek, G. E.; Trantolo, D. J.; Cooper, T. M.; Gresser, J. D., Eds.; Marcel Dekker: New York, 1998; Chapter 28, p 983.
- (9) (a) Akagi, K.; Piao, G.; Kaneko, S.; Sakamaki, K.; Shirakawa, H.; Kyotani, M. *Science* **1998**, *282*, 1683. (b) Akagi, K.; Guo, S.; Mori, T.; Goh, M.; Piao, G.; Kyotani, M. *J. Am. Chem. Soc.* **2005**, *127*, 14647. (c) Goh, M.; Kyotani, M.; Akagi, K. *J. Am. Chem. Soc.* **2007**, *129*, 8519. (d) Goh, M.; Matsushita, T.; Kyotani, M.; Akagi, K. *Macromolecules* **2007**, *40*, 4762. (e) Mori, T.; Kyotani, M.; Akagi, K. *Macromolecules* **2008**, *41*, 607. (f) Kyotani, M.; Matsushita, S.; Nagai, T.; Matsui, Y.; Shimomura, M.; Kaito, A.; Akagi, K. *J. Am. Chem. Soc.* **2008**, *130*, 10880. (g) Mori, T.; Sato, T.; Kyotani, M.; Akagi, K. *Macromolecules* **2009**, *42*, 1817. (h) Goh, M.; Piao, G.; Kyotani, M.; Akagi, K. *Macromolecules* **2009**, *42*, 8590.
- (10) (a) Akagi, K. *Handbook of Conducting Polymers, Conjugated Polymers*, 3rd ed.; Skotheim, T. A.; Reynolds, J. R., Eds.; CRC Press: New York, 2007; pp 3–14. (b) Akagi, K. *Chem. Rev.* **2009**, *109*, 5354.
- (11) (a) Li, B. S.; Cheuk, K. K. L.; Salhi, F.; Lam, J. W. Y.; Cha, J. A. K.; Xiao, X.; Bai, C.; Tang, B. Z. *Nano Lett.* **2001**, *1*, 323. (b) Li, B. S.; Cheuk, K. K. L.; Ling, L.; Chen, J.; Xiao, X.; Bai, C.; Tang, B. Z. *Macromolecules* **2003**, *36*, 77. (c) Cheuk, K. K. L.; Lam, J. W. Y.; Chen, J.; Lai, L. M.; Tang, B. Z. *Macromolecules* **2003**, *36*, 5947.
- (12) (a) Friedel, G. *Ann. Phys.* **1922**, *18*, 273. (b) Buckingham, A. D.; Ceasar, G. P.; Dunn, M. B. *Chem. Phys. Lett.* **1969**, *3*, 540.
- (13) (a) Heppke, G.; Löttsch, D.; Oestreicher, F. Z. *Naturforsch., A: Phys. Sci.* **1986**, *41*, 1214. (b) Kanazawa, K.; Higuchi, I.; Akagi, K. *Mol. Cryst. Liq. Cryst.* **2001**, *364*, 825. (c) Rokunohe, J.; Yoshizawa, A. *J. Mater. Chem.* **2005**, *15*, 275.
- (14) (a) Gottarelli, G.; Mariani, P.; Spada, G. P.; Samori, B.; Forni, A.; Solladie, G.; Hibert, M. *Tetrahedron* **1983**, *39*, 1337. (b) *Chirality in Liquid Crystals (Partially Ordered Systems)*; Kitzerow, H. S., Bah, C., Eds.; Springer: New York, 2001.
- (15) (a) Eelkema, R.; Feringa, B. L. *J. Am. Chem. Soc.* **2005**, *127*, 13480. (b) Eelkema, R.; Feringa, B. L. *Org. Lett.* **2006**, *8*, 1331.
- (16) (a) Yorozyua, S.; Osaka, I.; Nakamura, A.; Inoue, Y.; Akagi, K. *Synth. Met.* **2003**, *135–136*, 93. (b) Oh-e, M.; Yokoyama, H.; Yorozyua, S.; Akagi, K.; Belkin, M. A.; Shen, Y. R. *Phys. Rev. Lett.* **2004**, *93*, 267402. (c) Kang, S. W.; Jin, S. H.; Chien, L. C.; Sprunt, S. *Adv. Funct. Mater.* **2004**, *14*, 329. (d) Goto, H.; Akagi, K. *Angew. Chem., Int. Ed.* **2005**, *44*, 4322. (e) Goto, H.; Akagi, K. *Chem. Mater.* **2006**, *18*, 255.
- (17) (a) Goto, H.; Akagi, K. *Macromol. Rapid Commun.* **2004**, *25*, 1482. (b) Goto, H.; Akagi, K. *Macromolecules* **2005**, *38*, 1091. (c) Goto, H.; Nomura, N.; Akagi, K. *J. Polym. Sci., Part A: Polym. Chem.* **2005**, *43*, 4298. (d) Hayasaka, H.; Tamura, K.; Akagi, K. *Macromolecules* **2008**, *41*, 2341.
- (18) de Gennes, P. G.; Prost, J. *The Physics of Liquid Crystal*; Oxford University Press: Oxford, 1995.
- (19) Demus, D.; Goodby, J.; Gray, G. W.; Spiess, H.-W.; Vill, V. *Handbook of Liquid Crystals Vol. 1: Fundamentals*; Wiley-VCH: Weinheim, Germany, 1998.
- (20) (a) Gottarelli, G.; Samori, B.; Stremmenos, C.; Torre, G. *Tetrahedron* **1981**, *37*, 395. (b) Grandjean, F. C. *Acad. Sci.* **1921**, *172*. (c) Cano, R. *Bull. Soc. Fr. Mineral.* **1968**, *91*, 20.
- (21) Morrison, R. T.; Boyd, R. N. In *Organic Chemistry*, 5th ed.; Tokyo Kagaku Dojin: Tokyo, 1989; pp 164–166.
- (22) (a) Finkelmann, H.; Stegemeyer, H. Z. *Naturforsch., A: Phys. Sci.* **1973**, *28*, 799. (b) Finkelmann, H.; Stegemeyer, H. *Ber. Bunsen-Ges.* **1978**, *82*, 1302.
- (23) (a) Heppke, G.; Oestreicher, F. *Mol. Cryst. Liq. Cryst., Lett. Sect.* **1978**, *41*, 245. (b) Uchida, T.; Inukai, T. In *Liquid Crystal-Fundamentals*; Okano, K., Kobayashi, S., Eds.; Baifu-kan: Tokyo, 1985; pp 205–231.
- (24) (a) Araya, K.; Mukoh, A.; Narahara, T.; Shirakawa, H. *Synth. Met.* **1986**, *4*, 199. (b) Akagi, K.; Shirakawa, H.; Araya, K.; Mukoh, A.; Narahara, T. *Polym. J.* **1987**, *19*, 185. (c) Akagi, K.; Katayama, S.; Shirakawa, H.; Araya, K.; Mukoh, A.; Narahara, T. *Synth. Met.* **1987**, *17*, 241. (d) Akagi, K.; Katayama, S.; Ito, M.; Shirakawa, H.; Araya, K. *Synth. Met.* **1989**, *28*, D51. (e) Sinclair, M.; Moses, D.; Akagi, K.; Heeger, A. J. *Phys. Rev. B: Condens. Matter Mater. Phys.* **1988**, *38*, 10724.
- (25) (a) Montaner, A.; Rolland, M.; Sauvajol, J. L.; Galtier, M.; Almairac, R.; Ribet, J. L. *Polymer* **1988**, *29*, 1101. (b) Coustel, N.; Foxon, N.; Ribet, J. L.; Bernier, P.; Fischer, J. E. *Macromolecules* **1991**, *24*, 5867.
- (26) <http://en.wikipedia.org/wiki/File:Gear-kegelzahnrad.svg>. Accessed Jan 30, 2010.
- (27) Matsushita, T.; Goh, M.; Kyotani, M.; Akagi, K. *Curr. Appl. Phys.* **2006**, *6*, 952. (b) Goh, M.; Matsushita, T.; Satake, H.; Kyotani, M.; Akagi, K. *Macromolecules* **2010**, *43*, 5943.